HHS Public Access

Author manuscript

Nat Struct Mol Biol. Author manuscript; available in PMC 2021 January 13.

Published in final edited form as:

Nat Struct Mol Biol. 2020 September ; 27(9): 781–789. doi:10.1038/s41594-020-0458-9.

A redox switch regulates the structure and function of anti-apoptotic BFL-1

Kyle J. Korshavn[1,2], **Thomas E. Wales**[3], **Gregory H. Bird**[1,2], **John R. Engen**[3], **Loren D. Walensky**[1,2]

[1]Department of Pediatric Oncology, Dana-Farber Cancer Institute, Boston, Massachusetts, USA

[2]Linde Program in Cancer Chemical Biology, Dana-Farber Cancer Institute, Boston, Massachusetts, USA

[3]Department of Chemistry and Chemical Biology, Northeastern University, Boston, Massachusetts, USA

Abstract

Apoptosis is regulated by BCL-2 family proteins. Anti-apoptotic members suppress cell death by deploying a surface groove to capture the critical BH3 α-helix of pro-apoptotic members. Cancer cells hijack this mechanism by overexpressing anti-apoptotic BCL-2 family proteins to enforce cellular immortality. We previously identified and harnessed a unique cysteine (C55) in the groove of anti-apoptotic BFL-1 to selectively neutralize its oncogenic activity using a covalent stapled-peptide inhibitor. Here, we find that disulfide-bonding between a native cysteine pair at the groove (C55) and C-terminal α9 helix (C175) of BFL-1 operates as a redox switch to control the accessibility of the anti-apoptotic pocket. Reducing the C55-C175 disulfide triggers α9 release, which promotes mitochondrial translocation, groove exposure for BH3 interaction, and inhibition of mitochondrial permeabilization by pro-apoptotic BAX. C55-C175 disulfide-formation in an oxidative cellular environment abrogates the ability of BFL-1 to bind BH3 domains. Thus, we identify a mechanism of conformational control of BFL-1 by an intramolecular redox switch.

INTRODUCTION

BCL-2 family proteins are master regulators of mitochondrial apoptosis and control cell fate in response to stress through protein-protein and protein-membrane interactions[1,2]. Although BCL-2 family proteins share a series of BCL-2 homology (BH) domains, only the pro-apoptotic multi-BH domain members, such as BAX and BAK, can self-associate to disrupt the integrity of the mitochondrial outer membrane, discharging signaling factors that

Corresponding Author: Loren D. Walensky, loren_walensky@dfci.harvard.edu.

AUTHOR CONTRIBUTIONS

K.J.K. and L.D.W. designed the study; K.J.K. produced the BFL-1 proteins and performed all biochemical, mitochondrial, and cellular experiments. G.H.B. generated peptides. K.J.K. and T.E.W. performed the HXMS analyses under the supervision of J.R.E. L.D.W. and K.J.K. wrote the manuscript, which was reviewed by all co-authors.

COMPETING INTERESTS STATEMENT

L.D.W. is a scientific co-founder and shareholder in Aileron Therapeutics.

catalyze the proteolytic caspase cascade[3,4]. The BH3 helix of BAX and BAK are required for homo-oligomerization and mitochondrial membrane permeabilization[5], and thus a key mechanism of apoptotic blockade involves the capture of these exposed BH3 helices in a groove located on the surface of anti-apoptotic proteins[6]. This heterodimeric helix-in-groove interaction informed the development of canonical groove inhibitors to block anti-apoptotic proteins and restore BAX and BAK-mediated mitochondrial apoptosis in human cancer[7]. Another class of pro-apoptotic BCL-2 family proteins display homology in the BH3 domain only and induces mitochondrial apoptosis by (1) activating-the-activators through a direct binding interaction with BAX or BAK and/or (2) inhibiting-the-inhibitors through targeting the canonical groove of anti-apoptotic members[8]. Ultimately, the relative balance of inhibitory and activating interactions determine the threshold for BAX and BAK homo-oligomerization, a critical control point of cell fate.

Given the gravity of the cell's life-death decision, a complex network of post-translational regulation exists to fine tune the structure and function of BCL-2 family proteins. Classic examples of BCL-2 protein modification include proteolytic cleavage, phosphorylation, and ubiquitination. For example, caspase-8 cleavage of BID yields tBID, a potent BH3-only activator of BAX and BAK and inhibitor of anti-apoptotic proteins[9], the phosphorylation status of the BH3-only protein BAD toggles its function between apoptotic and metabolic regulation[8], and the constitutive ubiquitination and proteasomal degradation of anti-apoptotic MCL-1 underlies its rapid turnover[10]. Less is known about the relative influence of cysteine post-translational modifications in BCL-2 family biology, although several examples have been reported. For example, enzymatic palmitoylation and non-enzymatic trans-2-hexadecenal lipidation of BAX at C126 enhances mitochondrial translocation and pro-apoptotic function[11,12], oxidation of BAX at C62 induces conformational activation[13], oxidation of BCL-2 at C158 and C229 reduces the apoptotic threshold in human lung epithelial cells[14], and S-nitrosylation of BCL-2 at C158 and C229 stabilizes the protein by impairing ubiquitin-proteasomal degradation[15]. Small molecule and stapled-peptide covalent modification of discrete cysteine residues in BCL-2 family proteins have further revealed conformational effects with functional implications. Whereas small molecule derivatization of MCL-1 at C286 disrupted the BH3-binding activity of the canonical groove by an allosteric mechanism[16], direct targeting of a unique cysteine (C55) in the surface groove of BFL-1 by a cysteine-reactive stapled peptide selectively neutralized its anti-apoptotic activity and reactivated apoptosis in BFL-1-driven cancers[17–19]. Thus, characterizing the diverse mechanisms of BCL-2 family post-translational regulation is not only essential to our fundamental understanding of apoptotic signaling, but can also inform the development of pharmacologic strategies to modulate the apoptotic threshold in human disease.

Dissecting the biochemistry and structure of BCL-2 family proteins has predominantly relied on studying recombinant proteins that lack the α9 transmembrane helix, due to the expression and purification complications linked to its hydrophobic character. Indeed, the fundamental discovery of the BH3-in-groove binding mode and the subsequent development of therapeutic inhibitors were successfully accomplished using α9-truncated proteins[6]. Likewise, our studies of selective BFL-1 inhibition by targeting a cysteine exclusively found in the surface groove of BFL-1, were accomplished using α9-truncated BFL-1 (BFL-1ΔC)[17–19]. This "pocket-exposed" form may in fact mirror the functionally relevant

structure of anti-apoptotic BCL-2 family proteins at the mitochondrial membrane, where α9 membrane insertion by definition reflects its release from the canonical groove, exposing the critical surface for BH3 interaction. Intriguingly, we found that complementary cysteine pairing between C55 of BFL-1ΔC and C25 of NOXA BH3 enabled disulfide-bond formation, providing the first example of BH3-in-groove inhibition of an anti-apoptotic protein by covalent reaction[19]. This natural disulfide inspired the replacement of NOXA C25 with an electrophilic warhead, which in addition to hydrocarbon-stapling to stabilize BH3 α-helical structure, yielded a potent and exquisitely selective covalent inhibitor of BFL-1[17,19]. Here, by generating and characterizing full-length recombinant BFL-1 protein, we identified a native cysteine within the α9 helix itself that is capable of intramolecular disulfide-bond formation with C55, revealing an unprecedented mode of anti-apoptotic protein regulation by a redox switch.

RESULTS

Selective disulfide bond formation between C55 and C175 of anti-apoptotic BFL-1

Structural analyses of full-length BCL-2 proteins, such as BAX, BCL-X_L, and BCL-w, indicate that α9 can engage in intramolecular interaction with the canonical BH3-binding groove[20–22]. In the absence of a full-length BFL-1 structure, we hypothesized that C55 within the groove could potentially engage one of two cysteines, C165 or C175, in the α9 helix, and thereby enable the formation of a disulfide bridge. Indeed, homology modeling using I-TASSER[23–25] indicated that a complementary α9-in-groove interaction was feasible, yielding a calculated structure similar to the crystal structure of the complex between NOXA BH3 and BFL-1ΔC (PDB ID: 3MQP) (Fig. 1a). In the absence of constraints, the model structure further predicted an intramolecular disulfide between C55 and C175. Interestingly, in examining the evolutionary conservation of cysteines in the BFL-1 protein, C55 initially arose during the transition from birds to reptiles, whereas C165 arose later in placental mammals. Intriguingly, C175 is found exclusively in higher order primates and only occurs when C55 is also present, suggesting an evolution-function correlation rarely seen for redox switches (Fig. 1b, Supplementary Data File 1)[26]. These cysteines are absent in rodent BFL-1 homologues, an important consideration when vetting C55-targeting covalent BFL-1 inhibitors in model organisms for clinical development.

To verify if disulfide-bond formation occurs between α9 and the groove in the context of full-length BFL-1 protein and determine the relevant cysteine partners, we first developed a protocol to robustly generate pure, full-length human BFL-1 protein and a series of cysteine mutants (Extended Data Fig. 1) for probing the reactivity of C55-C165 vs. C55-C175 pairings. The generated constructs, C4S/C19S (bearing C55/C165/C175), C4S/C19S/C175S (bearing C55/C165), C4S/C19S/C165S (bearing C55/C175), and C4S/C19S/C55S/C165S/C175S (bearing no cysteines), were then analyzed by gel electrophoresis in the presence and absence of reducing agent (dithiothreitol, DTT). Strikingly, only those constructs containing both C55 and C175 demonstrated a faster-migrating species in the absence of reducing agent, indicative of selective, intramolecular disulfide-bond formation, which yields a more compact protein with decreased hydrodynamic surface area[27] (Fig. 1c). Thus, the reductive analyses of full-length BFL-1 proteins revealed that a disulfide bond naturally forms

between α9 and the BH3-binding groove of BFL-1 upon recombinant protein expression and purification, and is specific to the C55-C175 pair, consistent with the calculated model structure.

Conformational consequences of the α9 redox switch

We applied hydrogen-deuterium exchange mass spectrometry (HXMS) to examine the impact of reversible disulfide bond formation between α9 and the canonical pocket on the conformational dynamics of BFL-1. HXMS probes protein structure by measuring the deuterium incorporation of backbone amide hydrogens. When diluted into deuterium buffer, backbone hydrogens of flexible and/or exposed protein regions rapidly exchange with deuterium. In contrast, buried domains and/or those regions that contain hydrogen-bonding of backbone amide hydrogens (such as in α-helices), or that are engaged in ligand interactions, demonstrate slowed or suppressed deuterium exchange. We first determined the deuterium uptake profiles of BFL-1 lacking its α9 helix and bearing C4S/C19S mutations (retains only C55; hereafter referred to as BFL-1ΔC C55) and full-length BFL-1 C4S/C19S/C165S (retains C55/C175; hereafter referred to as BFL-1 C55/C175), in the presence and absence of β-mercaptoethanol (BME) at 10 seconds and 10 minutes of deuterium labeling. Time-dependent deuterium exchange was most evident in the regions spanning amino acids 18–66, encompassing the flexible α1-α2 loop and α-helices 2–4, and in the C-terminal region from the distal portion of α8 through the C-terminus (aa 144–175) (Extended Data Fig. 2, Supplementary Table 1, and Supplementary Data File 2). The α9 segment of the full-length form was rapidly deuterated, indicative of only minor hydrogen bonding protecting backbone amide hydrogens. In contrast, the α5/α6 hydrophobic core of the protein showed relatively less deuterium exchange, and the N-terminal region containing α1 was especially well protected. These changes are consistent with the overall fold of C-terminally truncated BFL-1 protein as determined by X-ray crystallography[18,28], and full-length homologs of BFL-1, such as BAX and BCL-w, as determined by nuclear magnetic resonance (NMR) spectroscopy[20,29]. The uptake profiles further suggest that α2-α4 and α9, which either form or engage the canonical BH3-binding groove, respectively, exhibit conformational flexibility in both the presence and absence of reducing agent, which may be important for accommodating the helix-in-groove interactions that underlie BCL-2 family functionality.

With these HXMS profiles in hand, we next calculated the differences in deuterium uptake between (1) BFL-1ΔC C55 and BFL-1 C55/C175, and (2) BFL-1 C55/C175 in the presence and absence of reducing conditions, to determine the influence of α9 residues and their disposition on the structure of BFL-1. In the absence of α9 (BFL-1ΔC C55), there was relative deprotection of α-helices 2 and 3, which contribute to the surface of the BFL-1 BH3-binding groove (Fig. 2a–c, Supplementary Table 1, and Supplementary Data File 2). These data are consistent with engagement of the canonical groove by residues of α9 in the context of full-length BFL-1 C55/C175, resulting in relative protection of the α2 and α3 helical surfaces. Strikingly, when full-length BFL-1 C55/C175 was treated with reducing agent (BME), the very region that showed relative deprotection in BFL-1ΔC C55 was likewise more exposed in BFL-1 C55/C175 (Fig. 2d–e, Supplementary Table 1, and Supplementary Data File 2). That is, reduction of the C55-C175 disulfide bond resulted in sufficient mobilization of α9 residues from the canonical pocket to enable deprotection of

the α2 and α3 surfaces comparable to BFL-1ΔC C55. Thus, despite the notably flexible conformation of α9, as evidenced by rapid deuterium exchange in the presence or absence of reducing agent, disulfide formation tethers α9 residues in a manner that obstructs the groove. These data highlight that the redox state of C55/C175 dictates both the disposition of α9 residues and access to the canonical pocket, suggestive of a conformational switch that can turn off or turn on the critical BH3-binding functionality of anti-apoptotic BFL-1.

Impact of the α9 redox switch on the stability and BH3-binding activity of BFL-1

The differential electrophoretic mobility and HXMS profiles of full-length BFL-1 bearing an oxidized or reduced C55/C175 pair suggested that redox state could influence the biophysical and biological properties of BFL-1. To assess comparative protein stability, we performed differential scanning fluorimetry (DSF) analyses of BFL-1ΔC C55, full-length BFL-1 C55/C175, and full-length cysteine-free BFL-1 (hereafter referred to as BFL-1 Cys-free), in the absence and presence of reducing conditions (10 μM, 100 μM BME). BFL-1ΔC C55 demonstrated a thermal stability profile that was independent of redox state (T_m, 51–52°C across all conditions), consistent with the absence of α9 and C175 (Fig. 3a, Table 1, Supplementary Data File 3). In contrast, full-length BFL-1 C55/C175 was substantially more stable than BFL-1ΔC C55 in the absence of BME (T_m, 65°C), and became progressively more unstable with increasing concentrations of added BME, as demonstrated by a shift of the denaturation curve to the left and correspondingly lower T_ms (Fig. 3b, Table 1, Supplementary Data File 3). Interestingly, BFL-1 Cys-free manifested a thermal stability profile under all conditions that matched the denaturation curve and T_m of maximally-reduced BFL-1 C55/C175 (Fig. 3c, Table 1, Supplementary Data File 3), reflecting structural similarity of the two constructs under conditions where α9 disulfide tethering is either not an option (BFL-1 Cys-free) or fully reduced (BFL-1 C55/C175, 100 μM BME). These data demonstrate that the presence of the C55-C175 disulfide bond stabilizes BFL-1 in solution, consistent with a more compact globular conformation, whereas reduction of the disulfide bond dose-responsively destabilizes the protein, due to the relative release of the hydrophobic α9 helix from its hydrophobic pocket.

To examine the impact of canonical groove accessibility on BH3-binding activity, we evaluated the three BFL-1 constructs in the presence and absence of reducing conditions by fluorescence polarization (FP) assays using FITC-derivatized BID BH3 peptide, a broad spectrum BH3 ligand that binds to anti-apoptotic members and can directly activate BAX[1]. Consistent with the thermal stability of BFL-1ΔC C55, relatively stable and high affinity BID BH3-binding activity (K_d, 1.6–24 nM) was observed upon exposure to escalating concentrations of BME (Fig. 3d, Table 2, Supplementary Data File 3). In contrast, full-length BFL-1 C55/C175 showed no FITC-BID BH3 binding activity in the absence of BME but progressively increased affinity upon BME titration (Fig. 3e, Table 2, Supplementary Data File 3). Of note, even at the highest BME dose tested, the BH3-binding activity of BFL-1 C55/C175 was 160-fold lower than that observed for BFL-1ΔC C55. Finally, for BFL-1 Cys-free, BH3-binding affinity was stable across all conditions and comparatively weaker than that measured for BFL-1ΔC C55 by 3–35 fold, consistent with binding interference from the mobile α9 helix (as observed previously for other anti-apoptotic proteins such as BCL-X_L[30]) but still achieving K_ds in the 55–90 nM range (Fig. 3f, Table 2,

Supplementary Data File 3). At the highest BME concentration tested, BFL-1 C55/C175 binding activity improved from undetectable to 260 nM, but this was still 5-fold lower than that observed for BFL-1 Cys-free (56 nM) under the same conditions. Taken together, these data demonstrate that C55-C175 disulfide formation completely blocks BH3 interaction, which is gradually restored upon chemical reduction. Because the capacity to engage pro-apoptotic BH3 domains underlies the anti-apoptotic activity of BCL-2 family proteins such as BFL-1, these results highlight the potential functional consequences of a redox switch that controls the location of α9 in BFL-1.

BFL-1 inhibition of BAX-mediated membrane permeabilization is regulated by the disposition of its α9 residues

To directly interrogate the functional consequences of a redox switch that dictates the conformational disposition of α9 in BFL-1, we compared the capacity of BFL-1ΔC C55, BFL-1 C55/C175, and BFL-1 Cys-free (0–500 nM) to block tBid-activated (20 nM), BAX-mediated (500 nM) membrane poration in a liposomal release assay[31], in the presence and absence of reducing conditions. As in the BH3-peptide binding assay, the ability of BFL-1ΔC C55 to engage pro-apoptotic BH3 helices, such as those of tBID and BAX, and dose-responsively suppress BAX-mediated membrane poration was unaffected by the addition of BME (Fig. 4a–b). In contrast, full-length BFL-1 C55/C175 demonstrated remarkably impaired BAX-inhibitory activity (Fig. 4c), which was restored by the addition of BME (Fig. 4d). Like BFL-1ΔC C55, the BAX-suppressive activity of BFL-1 Cys-free was not altered by redox conditions (Fig. 4e–f). These data demonstrate that toggling BFL-1 C55/C175 between a covalent and non-covalent α9-in-groove state directly influences the capacity of BFL-1 to block BH3-triggered BAX activation.

We next examined the influence of disulfide-bond formation between α9 and the canonical groove on BFL-1 translocation to isolated BAX/BAK-deficient mouse liver mitochondria. We incubated BFL-1ΔC C55, BFL-1 C55/C175, or BFL-1 Cys-free with mitochondria in the presence and absence of BME, followed by separation of the supernatant and mitochondrial pellet, and western analysis for BFL-1 and cytochrome *c*, which served as a mitochondrial marker. Whereas BFL-1ΔC C55, which lacks the α9 transmembrane domain helix, remained strictly in the supernatant fraction irrespective of redox conditions, full-length BFL-1 C55/C175 was predominantly found in the supernatant in the absence of BME but translocated to the mitochondrial fraction in the presence of BME (Fig. 5a–b). BFL-1 Cys-free, which bears an α9 that is otherwise not constrained by disulfide tethering, translocated to the mitochondrial fraction in the presence or absence of BME and to a similar extent observed for BME-treated BFL-1 C55/C175 (Fig. 5a–b). These data are consistent with previous cellular results showing the cytosolic disposition of expressed BFL-1ΔC but mitochondrial localization of full-length BFL-1[32], and further demonstrate that C55-C175 disulfide formation controls the relative distribution of BFL-1 between the supernatant and mitochondrial fraction as dictated by the disposition of its α9 domain.

To investigate the functional consequences of the BFL-1 α9 redox switch in the context of mitochondrial outer membrane permeabilization (MOMP), we incubated BAX/BAK-deficient mouse liver mitochondria with tBID (10 nM), BAX (100 nM), and the various

BFL-1 constructs (100 nM) in the presence and absence of BME (50 μM). Consistent with their differential capacity for mitochondrial targeting, BFL-1ΔC C55 was only modestly effective at blocking tBID-triggered, BAX-mediated cytochrome *c* release, whereas full-length BFL-1 Cys-free completely suppressed mitochondrial release activity, with both sets of results completely unaffected by the presence or absence of BME (Fig. 5c). In contrast, in the absence of BME, BFL-1 C55/C175 showed only weak BAX-inhibitory activity, equivalent to that of BFL-1ΔC, but upon addition of BME became as effective as BFL-1 Cys-free in blocking BAX-mediated cytochrome *c* release (Fig. 5c). These data highlight that the combined impact of covalent α9-in-groove engagement on mitochondrial localization and BH3-accessibility has a powerful influence on the functional capacity of BFL-1 to block BAX-mediated MOMP.

A redox switch controls BH3-binding by BFL-1 in cells

Finally, we sought to determine if the C55-C175 switch is operational in cells and can influence the BH3-binding functionality of BFL-1 in response to an oxidative stimulus. We took advantage of our cell-penetrant, C55-specific, covalent stapled BH3 inhibitor of BFL-1, D-NA-NOXA SAHB-15 R31E[17], which we deployed as a targeted thiol labeling reagent to probe the BH3-binding capacity of BFL-1 in cells. We expressed BFL-1ΔC C55, BFL-1 C55/C175, and BFL-1 Cys-free as N-terminal GFP-fusions in 293T cells, followed by treatment with biotinylated D-NA-NOXA SAHB-15 R31E under reducing (untreated) and oxidative (sub-cytotoxic hydrogen-peroxide treatment) conditions (Extended Data Fig. 3). Covalent BH3-engagement of the BFL-1 canonical pocket was then detected by biotin pull-down from cellular lysates and anti-GFP western analysis. First, we demonstrated that D-NA-NOXA SAHB-15 R31E labeled BFL-1ΔC C55 in the presence or absence of hydrogen-peroxide, confirming that the BFL-1 groove remains accessible under oxidizing conditions and that BFL-1 C55 in particular is still reactive and thus not oxidized (Fig. 5d–e). Whereas expressed BFL-1 C55/C175 likewise underwent covalent labeling by D-NA-NOXA SAHB-15 R31E in the reducing environment of untreated cells, hydrogen-peroxide exposure abrogated BFL-1 derivatization (Fig. 5d–e). This striking result suggests that the capacity to form a C55-C175 disulfide that locks α9 in place under oxidizing conditions can indeed occlude the canonical groove of BFL-1 and block BH3 capture. To confirm that the observed redox switch, as reflected by the conspicuous change in labeling, was indeed C55-dependent, the cellular experiment was repeated with expressed BFL-1 Cys-free protein and no BFL-1 derivatization was observed under any of the treatment conditions (Fig. 5d–e). Taken together, these data demonstrate that the BH3-binding ability of BFL-1, which explicitly dictates its anti-apoptotic functionality, can be directly influenced by the presence or absence of a disulfide bridge between C55 of the canonical groove and C175 of its C-terminal helix.

DISCUSSION

BFL-1 is a relatively understudied anti-apoptotic BCL-2 family member that has been implicated in the development and survival of granulocytes and lymphocytes, and upon pathologic overexpression can underlie autoimmune disease and cancer[33]. Interestingly, comprehensive deletion of BFL-1 isoforms in mice revealed only minor defects restricted to

the hematopoietic compartment, likely reflecting functional redundancy among BCL-2 family proteins and a therapeutic window for BFL-1 inhibition in cancer[34]. Indeed, BFL-1 has been implicated in the pathogenesis of melanoma, leukemia, and lymphoma, and has emerged as a resistance factor in cancers treated with the selective BCL-2 inhibitor, venetoclax[35–39]. Despite the immediate clinical relevance of BFL-1 in cancer pathogenesis and resistance to treatment, little is known about its post-translational control, aside from the identification of multiple ubiquitination sites and its relatively short half-life (~60 min)[27,30]. Given the critical importance of BCL-2 family regulation of mitochondrial apoptosis during health and disease, a diversity of post-translational modifications exist to fine tune BCL-2 family structure and function[40], informing novel approaches to modulate BCL-2 proteins for therapeutic benefit.

In order to avoid potential toxicity from broad targeting of BCL-2 family proteins in cancer, as observed for the ABT-263-associated thrombocytopenia that occurred in the context of dual BCL-2/BCL-X_L blockade[41], a major emphasis has been placed on developing selective inhibitors, such as venetoclax[42] and S63845[43] that respectively target BCL-2 and MCL-1. In searching for a selectivity factor for targeting BFL-1, we identified the unique C55 in its canonical BH3-binding pocket, which was amenable to precision targeting using stapled-peptide inhibitors modeled after the NOXA BH3 sequence and equipped with an acrylamide-bearing warhead[17–19]. Indeed, the NOXA BH3 domain itself bears a C25 residue that, when bound to BFL-1, aligns with C55 in the groove to readily form a disulfide bond *in vitro*[19], suggesting that covalent inhibition of anti-apoptotic proteins by native motifs may occur in a sufficiently-permissive oxidative environment. These findings prompted us to explore a functional role for the natural cysteines embedded in BFL-1 α9, which is typically removed upon recombinant protein expression and structure-function analysis. Here, by developing a novel method for robust expression of full-length BFL-1, we examined the propensity of α9 to form an intramolecular covalent adduct with C55 and determined that C175 was the relevant partner upon disulfide-bond formation. We demonstrated that a reversible disulfide tether, which alternatively locks α9 in place or releases it for membrane translocation and exposure of the canonical groove, has the capacity to impose redox control over the BH3-binding functionality of anti-apoptotic BFL-1, a phenomenon observed in liposomes, isolated mitochondria, and in cells. Whereas release of α9 from its binding pocket in the reducing environment of the cell may facilitate anti-apoptotic activity at the mitochondria during homeostasis or oncogenesis, oxidative stress may enforce covalent entrapment of α9, resulting in blockade of BFL-1 function.

Cysteine residues and disulfide-bond formation play critical roles in protein structure and function, and participate in redox sensing and signal transduction cascades in cells[44,45]. For example, cysteine derivatization has been shown to influence the respective pro- and anti-apoptotic activities of BAX and MCL-1[11,16]. Whereas redox-active cysteines serve as switches for a large variety of proteins, redox-active disulfides are typically involved in allosteric regulation or function at the active sites of disulfide-catalyzing enzymes[44,45]. Here, we discovered a disulfide switch embedded within a critical site of protein-protein interaction involved in apoptotic regulation. We demonstrate that the covalent interaction between C55 and C175 mediates accessibility to the canonical BH3-binding groove. Interestingly, BFL-1 has three additional cysteine residues (C4, C19, and C165) that could

potentially participate in alternate modes of protein regulation. Strikingly, both a natural ligand of BFL-1, NOXA BH3, and the intramolecular α9 domain, can engage the functional pocket of BFL-1 in a manner that aligns either NOXA C25 or BFL-1 C175 for disulfide-bond formation with C55 of the canonical groove. No other BCL-2 family protein contains a cysteine at this key regulatory site. The unprecedented toggling between covalent and non-covalent helix-in-groove interaction implicates BFL-1 as a specialized redox sensor, whose functional activity is dictated by the exposure of a singular cysteine residue located within its BH3-binding groove. As evidenced by our covalent stapled peptide inhibitor approach to selective targeting of BFL-1 in cancer[17–19] and disulfide-tethering screen that identified covalent small molecule inhibitors of BFL-1[46], the natural reactivity of C55 provides a unique opportunity to develop electrophilic warhead-bearing drugs that mimic the post-translational regulation of BFL-1 and inactivate its anti-apoptotic functionality for therapeutic benefit.

METHODS

Methods and their associated references are available in the online version of the paper.

ONLINE METHODS

Recombinant protein expression and purification

Full-length human BFL-1 containing an N-terminal His_6-tag (N-His_6) and a C-terminal alanine insertion (A176) was cloned into the pTYB1 vector using NdeI and SapI restriction sites. Point mutations were performed by PCR-based mutagenesis (Q5 Site-Directed Mutagenesis Kit, New England BioLabs) and validated by DNA sequencing. N-His_6 BFL-1ΔC (1–151) and full-length BAX were expressed in *E. coli* as previously reported.[30,47] Full-length BFL-1 in the pTYB1 vector was expressed in *E. coli* following a protocol adapted from the production of BAX.[30] Specifically, transformed *E. coli* were cultured in Luria Broth containing ampicillin (0.1 g/L), grown to an OD of 0.6–0.8, and protein expression was induced by the addition of 1.0 mM isopropyl β-D-1-thiogalactopyranoside (IPTG) at 16°C overnight. Bacterial pellets were collected by centrifugation and then resuspended in lysis buffer (250 mM NaCl, 20 mM Tris, pH 7.2) containing complete protease-inhibitor tablets (1 tablet per 3 L culture; Roche, EDTA-free). The cell suspensions were then lysed using a chilled microfluidizer, centrifuged to remove insoluble debris, and applied to either Ni-NTA agarose (BFL-1ΔC; Qiagen) or chitin resin (BFL-1 and BAX). N-His_6 BFL-1ΔC was washed with a gradual imidazole gradient and eluted with lysis buffer containing 150 mM imidazole. Eluted N-His_6 BFL-1ΔC was subsequently dialyzed overnight into lysis buffer lacking imidazole, concentrated, and further purified by size exclusion chromatography (SEC) using a Superdex S-75 (GE Healthcare) gel filtration system. Recombinant, full-length BAX and N-His_6 BFL-1 were cleaved from the chitin resin by overnight incubation with 50 mM DTT (BAX) or 100 mM hydroxylamine (N-His_6 BFL-1) at 4°C. Cleaved proteins were then concentrated and purified by SEC using a Superdex S-75 (GE Healthcare) gel filtration system. Protein purity and identity was verified by Coomassie staining and western blot analysis using a mouse monoclonal anti-His_6

antibody (BFL-1ΔC and BFL-1; Abcam) or HRP-conjugated anti-BAX antibody (2D2, Santa Cruz Biotechnology).

Structural calculations

A structural model of full-length BFL-1 (1–175) was generated using the I-TASSER server[23–25]. Wild-type BFL-1 sequence was employed and no constraints were imposed on the modeling calculations.

Phylogenetic analysis

All annotated sequences for BFL-1 were acquired from UniProt and aligned to the human sequence (Q16548) using ClustalOMEGA (Supplementary Data File 1). The presence of C55, C165, and C175 (human numbering) in all aligned sequences was analyzed within a five amino acid window surrounding each cysteine of interest to allow for potential flexibility within each sequence. The analyzed sequences were subsequently mapped onto a phylogenetic tree using the Interactive Tree of Life (iTOL) server[48].

Disulfide analysis

Recombinant, full-length BFL-1 proteins (1 μM) bearing the indicated combinations of native cysteines (C55/C165/C175, C55/C165, C55/C175, and Cys-free) were incubated in the absence or presence of 1 mM DTT in PBS (Gibco) at 25°C for 1 hour. Samples were then mixed with non-reducing gel loading dye, separated by SDS-PAGE electrophoresis (12% Bis-Tris gel), and analyzed by western blot using a mouse monoclonal anti-His_6 antibody (Abcam).

Hydrogen deuterium exchange mass spectrometry

Hydrogen deuterium exchange experiments were performed as described previously[49], with additional details provided in Supplementary Table 1 and Supplementary Data File 2. BFL-1ΔC C55 or BFL-1 C55/C175 (30 pmol) in the absence or presence of β-mercaptoethanol (BME, 100,000 pmol) were incubated at 21°C for 10 minutes. Samples were then deuterated for either 10 seconds or 10 minutes in labeling buffer (see Supplementary Table 1) followed by addition of an equal volume of quench buffer. Using a Waters UPLC HDX manager system maintained at 0°C, quenched samples were digested at 15°C with a pepsin column and the resulting peptides underwent a 3 minute trap and desalting step using a VanGuard pre-column trap (2.1 × 5 mm, ACQUITY UPLC BEH C18, 1.7 μM) flowing at 100 μL/min. Peptides were then separated using an ACQUITY UPLC HSS T3, 1.8 μm, 1.0 × 50 mm analytical column (Waters Corporation) with a 5–35% gradient of acetonitrile (0.1 % formic acid) over 6 minutes at a flow rate of 100 μL/min. Mass spectra were acquired using a Synapt G2-Si (Waters) in MS^E (data independent acquisition) mode with 0.4 scans/second over a 50–2000 m/z range with ion mobility engaged. BFL-1 peptic peptides were identified with Protein Lynx Global Server (PLGS 3.0.1, Waters Corporation, RRID: SCR_016664) using undeuterated BFL-1 (Supplementary Table 1 and Supplementary Data File 2). Data analysis was performed using DynamX 3.0 (Waters Corporation), including determination of centroid masses for each isotopic distribution, generation of deuterium uptake plots, and comparison between experimental

states. Relative deuterium uptake for each peptide was determined by subtracting the average mass of the undeuterated peptide from the average mass of the deuterated peptide. Deuterium exchange was not corrected for back-exchange and thus expressed as relative deuterium incorporation[50]. The HXMS data have been deposited to the ProteomeXchange Consortium via the PRIDE[51] partner repository with the dataset identifier PXD016059.

Differential scanning fluorimetry

Recombinant BFL-1 constructs (5 μM; BFL-1ΔC C55, BFL-1 C55/C175, or BFL-1 Cys-free) were incubated with 0, 10, or 100 μM BME and 10x Sypro Orange (ThermoFisher) in a 96 well plate for 30 minutes at 25°C. Thermal melt curves were then acquired on a 7500 Fast Real-Time PCR System (Applied Biosystems) and, after a two-minute equilibration period at 25°C, the temperature was gradually increased from 25 to 100°C at a rate of 2°C per minute. The fluorescence of Sypro Orange was measured every minute (490 ± 10 nm excitation, 575 ± 10 nm emission). Each thermal melt curve was independently normalized, and all replicates (8 per condition) were averaged. The melting phase of each curve was calculated by a Boltzman sigmoidal fit to identify the inflection point of the denaturation curve corresponding to the T_m of the protein.

Fluorescence polarization binding assay

Direct FP binding assays were performed as described previously[52]. Recombinant BFL-1 proteins (20 μM; BFL-1ΔC C55, BFL-1 C55/C175, or BFL-1 Cys-free) were preincubated with BME (0, 1, 5, 10, or 25 mM) for one hour, followed by serial dilution into binding assay buffer (100 mM NaCl, 50 mM Tris, pH 8.0) in a 96 well plate. FITC-BID BH3 peptide[16] (60 nM final concentration) was then added and the mixture incubated in the dark for 30 minutes at 25°C. Fluorescence readings (485 nm excitation, 525 nm emission) were performed on a SpectraMax M5 microplate reader (Molecular Devices). Data were analyzed by nonlinear regression analysis using Prism software (GraphPad) to calculate dissociation constants (K_d).

Liposomal release assay

Liposomal release assays were performed as described previously[53]. Large unilamellar vesicles (LUVs) were prepared with a lipid composition of 48 mol% phosphatidylcholine, 28 mol% phosphatidylethanolamine, 10 mol% phosphatidylinositol, 10% dioleyl phosphatidylserine, and 4 mol% tetraoleoyl cardiolipoin (Avanti Polar Lipids). The lipid mixture was prepared from chloroform stocks, dried as a thin film by vacuum (1 mg total lipid), and stored under nitrogen at −80°C until use. Fluorescent 8-aminonaphthalene-1,3,6-trisulfonic acid (ANTS) (6.3 mg) and fluorescence quencher p-xylene-bis-pyridinium bromide (DPX) (19.1 mg) were added to the dried film and rehydrated with 1 mL of liposome buffer (200 mM KCl, 5 mM $MgCl_2$, 10 mM Hepes, pH 7.0). Following 5 freeze-thaw cycles, the hydrated lipid solution was extruded through a 100-nm membrane (Whatman) using an Avanti mini extruder. LUVs were subsequently isolated from free ANTS/DPX by gravity flow SEC using Sepharose CL-2B resin (Sigma Aldrich) and liposome buffer. LUVs (5 μL) were mixed with the indicated combinations of BFL-1 (0, 50, 250, or 500 nM), tBID (20 nM), and BAX (500 nM) in the absence or presence of 1 mM BME in a 384-well black flat bottom plate (Corning). Upon addition of BAX (F_0), the

change in ANTS fluorescence (355 nm excitation, 520 nm emission) was monitored at one-minute intervals. After three hours of incubation, Triton X-100 was added at a final concentration of 0.5% (vol/vol) to determine maximal release (F_{100}). Percent ANTS/DPX release was then calculated as $[(F-F_0)/(F_{100}-F_0)]x100$.

Purification of BAX/BAK-deficient mouse liver mitochondria

Liver mitochondria from *Alb-Cre*^{pos}*Bax*$^{f/f}$*Bak*$^{-/-}$ mice were isolated as described previously[30]. Harvested livers were sliced, washed with isolation buffer (250 μM sucrose, 0.1 mM EGTA, 10 mM Tris, pH 7.4), dounce homogenized, and the resultant suspension centrifuged for 10 minutes at 800 × *g* at 4°C to remove residual fatty tissue. Mitochondria were then pelleted by centrifugation for 10 minutes at 7000 × *g* at 4°C. The pellet was resuspended, rinsed in cold isolation buffer, and centrifuged for a second time for 10 minutes at 7000 × *g* at 4°C. The resultant pellet was resuspended in 1 mL of isolation buffer and total protein concentration was measured by BCA protein assay (Pierce). Following quantification, the mitochondrial suspension was centrifuged for 10 minutes at 7000 × *g* at 4°C and then resuspended in preservation buffer (300 mM trehalose, 10 mM KCl, 1 mM EGTA, 1 mM EDTA, 0.1% BSA, 10 mM Hepes, pH 7.7) at a final protein concentration of 50 mg/mL, flash frozen on dry ice, and stored at −80°C until use.

In vitro mitochondrial translocation

Frozen BAX/BAK-deficient mitochondria were thawed on ice and the buffer exchanged from storage buffer to experimental buffer (200 mM mannitol, 70 mM sucrose, 1 mM EDTA, 10 mM Hepes, pH 7.4) at a final protein concentration of 50 mg/mL. BFL-1 constructs (1 μM) in the absence or presence of 5 mM BME were incubated with mitochondria (4 mg/mL) at room temperature for 1 hour. After incubation, samples were centrifuged at 8000 × *g* for 15 minutes at 4°C and the supernatant was collected. The pelleted mitochondria were resuspended in an equal volume of mitochondrial experimental buffer supplemented with 1% (vol/vol) Triton X-100 to solubilize the mitochondrial fraction. Supernatant and mitochondrial fractions were then analyzed by SDS-PAGE and western blot using a mouse monoclonal anti-His_6 antibody (Abcam). Western analysis using a mouse monoclonal anti-cytochrome *c* antibody (Abcam) was also performed to both verify the mitochondrial fraction and ensure that the treatment protocol did not compromise mitochondrial membrane integrity.

Mitochondrial cytochrome *c* release assay

Frozen mitochondria were prepared, thawed, and buffer exchanged as described above. Mitochondria (1 mg/mL) were then incubated for one hour at 25°C with the indicated combination of BFL-1 construct (100 nM), BAX (100 nM), tBid (10 nM), and BME (50 μM) in a 96 well plate. Control wells contained mitochondria and buffer, with and without added 1% Triton X-100 (vol/vol). Following incubation, plates were centrifuged for 15 minutes at 3400 rpm and 50 μL of supernatant analyzed using the Rat/Mouse Cytochrome *c* Quantikine ELISA Kit (R&D Systems) according to the manufacturer's instructions. Percent cytochrome *c* released into the supernatant (%cyto *c* release) was calculated according to the following equation: %cyto *c* release = [cyto c_{sup} – cyto c_{buffer}]/ [cyto c_{max} – cyto c_{buffer}]*100, where cyto c_{sup} – cyto c_{buffer} and cyto c_{max} – cyto c_{buffer} represent the amount

of cytochrome *c* specifically released into the supernatant upon treatment with the indicated conditions or 1% (v/v) Triton X-100, respectively.

Cultured cell lines

293T cells (purchased from and authenticated by ATCC) were cultured in DMEM media that was supplemented with penicillin/streptomycin and 10% FBS. Cells were verified as mycoplasma-negative using the MycoAlert mycoplasma detection kit (Lonza Biologics).

Cell viability assay

293T cells were cultured as described above, plated in 96 well plates (5,000 cells per well), and allowed to adhere for 24 h. The cells were then treated with the indicated concentrations of H_2O_2 for 24 h. Cell viability was measured using CellTiter-Glo (Promega) with luminescence read on a Spectramax M5 microplate reader. Curve fitting was performed by nonlinear regression analysis using Prism software (Graphpad).

Cellular BH3-in-groove assay

293T cells at 70% confluence in 6-well plates were transiently transfected with 3 μg of eGFP plasmid containing N-terminal GFP-tagged BFL-1ΔC C55, BFL-1 C55/C175, or BFL-1 Cys-free constructs using Lipofectamine LTX & Plus reagent (ThermoFisher). The media was replaced 24 h following transfection, and after a 2 h recovery period, the cells were treated for 24 h with H_2O_2 (100 μM) and/or D-NA-NOXA SAHB-15 R31E[17] bearing a C-terminal biotin tag (5 μM). The cells were subsequently washed with PBS to remove any free peptide, harvested, and lysed with CHAPS buffer (50 mM Tris pH 7.4, 150 mM NaCl, 1% CHAPS [v/v]). Protein concentration of the soluble fraction was determined by BCA assay according to the manufacturer's protocol (Thermo Scientific). Biotin capture of the D-NA-NOXA SAHB/BFL-1 adduct was achieved by incubating 400 μg of lysate from each treatment condition, diluted into PBS, with high-capacity streptavidin agarose beads (Thermo Scientific) for 24 h at 4°C. The beads were then washed with 5 × 200 μL PBS and 3 × 200 μL 1% NP-40 in PBS. Bead-bound complex was eluted by boiling in 2x LDS containing 300 mM DTT. Samples were subjected to electrophoresis and western blotting using a GFP antibody (Invitrogen, CAB4211) to evaluate relative BH3-capture of GFP-BFL-1 protein.

Statistical Methods

Prism software (Graphpad) was used for data analysis, and calculating mean, S.D., S.E., T_m, and K_d values.

Reporting Summary Statement

Further information on experimental design is available in the Nature Research Reporting Summary linked to this article.

Data Availability Statement

HXMS data have been deposited to the PRIDE database with identifier code PXD016059. All data generated or analyzed for this study are included in this manuscript and its supplementary files. Source data are available with the paper online.

Extended Data

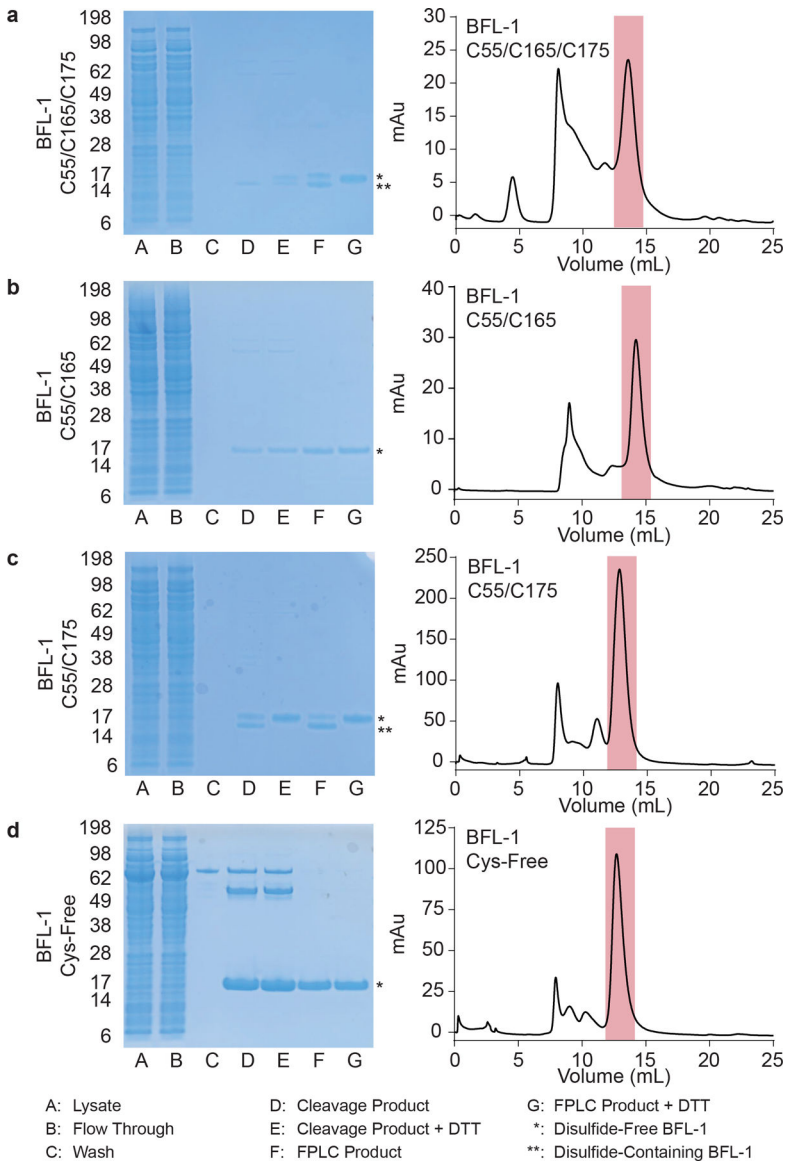

Extended Data Fig. 1. Purification of recombinant full-length BFL-1 constructs.

(a-d) The indicated full-length, N-His_6 BFL-1 constructs bearing a C-terminal chitin binding domain (CBD) were expressed in BL21 DE3 cells, purified by chitin affinity resin, subjected to overnight cleavage with hydroxylamine (100 mM), and further purified by SEC. Full-length BFL-1 constructs bearing C55 and C175 (a, c) were isolated as a doublet under non-reducing conditions and as a singlet under reducing conditions, as demonstrated by gel

electrophoresis and Coomassie stain. The shaded peak on the FPLC profile indicates the fraction containing pure, full-length BFL-1 protein.

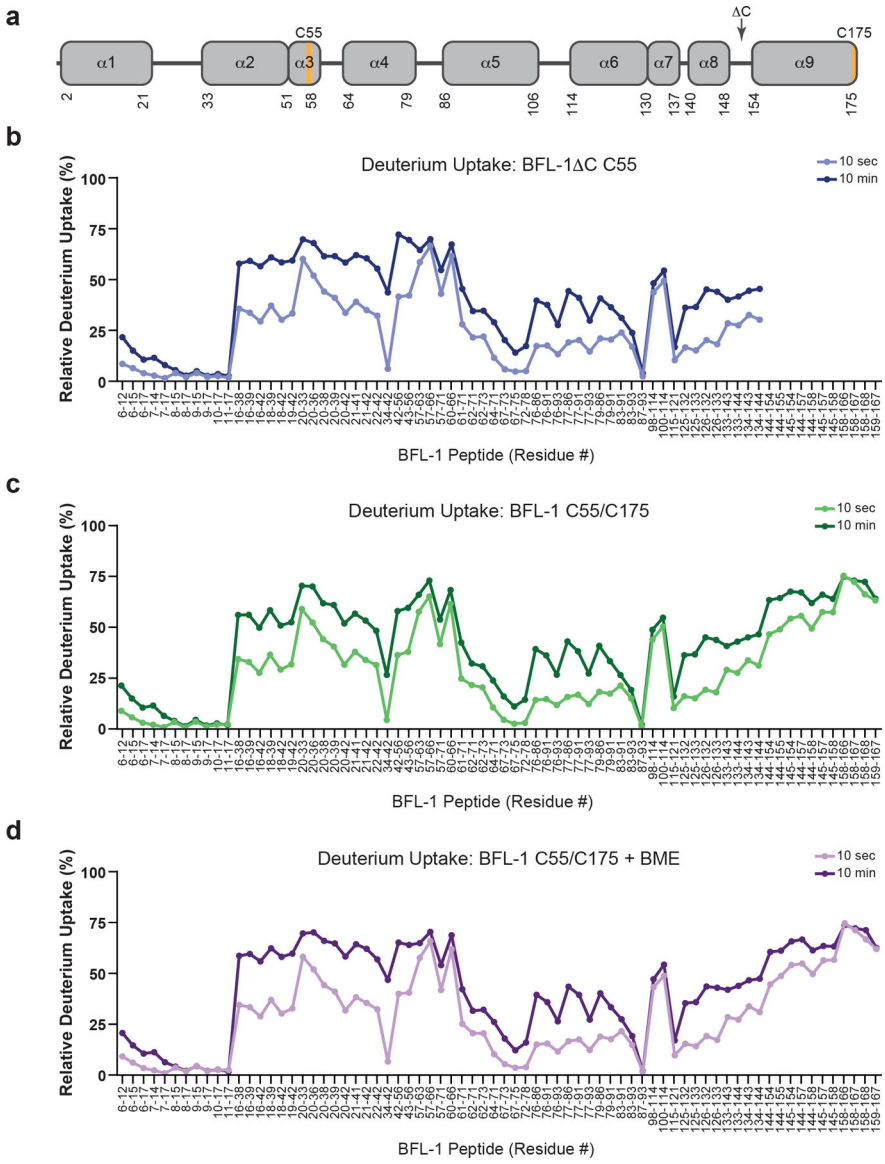

Extended Data Fig. 2. Hydrogen-deuterium exchange profiles of BFL-1ΔC C55 and BFL-1 C55/C175.

(a) Domain map of full-length BFL-1 highlighting the amino acid sequences that correspond to the individual α-helices, the truncation site for BFL-1ΔC C55, and the locations of C55 and C175 (colored in orange). (b-d) The deuterium uptake profiles of BFL-1ΔC C55 (b), BFL-1 C55/C175 without BME (c), and BFL-1 C55/C175 with BME (d) were measured at 10 seconds and 10 minutes of deuterium labeling. The relative deuterium uptake plots demonstrate significant time-dependent exchange in the region spanning the α1-α2 loop to the proximal portion of α4 helix (aa 18–66) and in the C-terminal region from the distal portion of α8 through the C-terminus (aa 144–175). The α5/α6 hydrophobic core of the protein showed relatively less deuterium exchange, and the N-terminal region containing α1

demonstrated little to no deuterium uptake. Data are representative of three independent experiments for BFL-1ΔC C55 and BFL-1 C55/C175 and two independent experiments for BME-reduced BFL-1 C55/C175 (see Supplementary Table 1). All HXMS data used to create this figure can be found in Supplementary Data File 2.

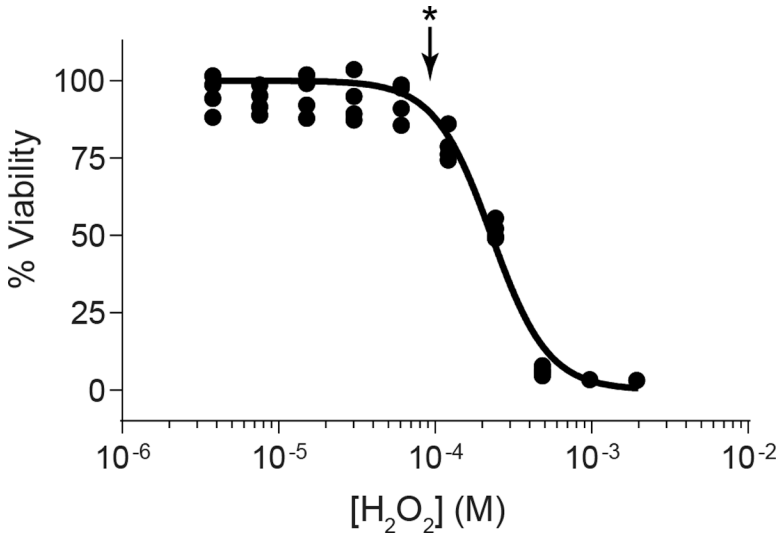

Extended Data Fig. 3. Cellular response to H_2O_2 treatment.

Cell viability of 293T cells treated with the indicated concentrations of H_2O_2 and measured at 24 h. Data are mean ± s.d. of four technical replicates. The experiment was repeated twice using independent cell cultures and treatments with similar results. The sub-cytotoxic dose of 100 μM (asterisk) was chosen for pull-down experiments (Fig. 5d–e). Data for the cell viability plot is available online.

Supplementary Material

Refer to Web version on PubMed Central for supplementary material.

ACKNOWLEDGMENTS

We thank E. Smith for assistance with figure preparation. The study was funded by NIH grant R35CA197583 and a Leukemia and Lymphoma Society Translational Research Program grant to L.D.W., an American Cancer Society Postdoctoral Fellowship Award to K.J.K, and NIH grant R50CA211399 to G.H.B. Additional support was provided by a research collaboration between J.R.E. and the Waters Corporation. We are also thankful to the Wolpoff Family Foundation, Jim and Lisa LaTorre, the family of Ivo Coll, and the Todd J. Schwartz Memorial Fund for their financial contributions to our cancer chemical biology research.

REFERENCES

1. Czabotar PE, Lessene G, Strasser A & Adams JM Control of apoptosis by the BCL-2 protein family: implications for physiology and therapy. Nat Rev Mol Cell Biol 15, 49–63 (2014). [PubMed: 24355989]
2. Leber B, Lin J & Andrews DW Still embedded together binding to membranes regulates Bcl-2 protein interactions. Oncogene 29, 5221–30 (2010). [PubMed: 20639903]
3. Kalkavan H & Green DR MOMP, cell suicide as a BCL-2 family business. Cell Death Differ 25, 46–55 (2018). [PubMed: 29053143]

4. Walensky LD & Gavathiotis E BAX unleashed: the biochemical transformation of an inactive cytosolic monomer into a toxic mitochondrial pore. Trends Biochem Sci 36, 642–52 (2011). [PubMed: 21978892]
5. Wang K, Gross A, Waksman G & Korsmeyer SJ Mutagenesis of the BH3 domain of BAX identifies residues critical for dimerization and killing. Mol Cell Biol 18, 6083–9 (1998). [PubMed: 9742125]
6. Sattler M et al. Structure of Bcl-xL-Bak peptide complex: recognition between regulators of apoptosis. Science 275, 983–6 (1997). [PubMed: 9020082]
7. Oltersdorf T et al. An inhibitor of Bcl-2 family proteins induces regression of solid tumours. Nature 435, 677–81 (2005). [PubMed: 15902208]
8. Letai A et al. Distinct BH3 domains either sensitize or activate mitochondrial apoptosis, serving as prototype cancer therapeutics. Cancer Cell 2, 183–92 (2002). [PubMed: 12242151]
9. Li H, Zhu H, Xu CJ & Yuan J Cleavage of BID by caspase 8 mediates the mitochondrial damage in the Fas pathway of apoptosis. Cell 94, 491–501 (1998). [PubMed: 9727492]
10. Zhong Q, Gao W, Du F & Wang X Mule/ARF-BP1, a BH3-only E3 ubiquitin ligase, catalyzes the polyubiquitination of Mcl-1 and regulates apoptosis. Cell 121, 1085–95 (2005). [PubMed: 15989957]
11. Cohen DT, Wales TE, McHenry MW, Engen JR & Walensky LD Site-Dependent Cysteine Lipidation Potentiates the Activation of Proapoptotic BAX. Cell Rep 30, 3229–3239 e6 (2020). [PubMed: 32160532]
12. Frohlich M, Dejanovic B, Kashkar H, Schwarz G & Nussberger S S-palmitoylation represents a novel mechanism regulating the mitochondrial targeting of BAX and initiation of apoptosis. Cell Death Dis 5, e1057 (2014). [PubMed: 24525733]
13. Nie C et al. Cysteine 62 of Bax is critical for its conformational activation and its proapoptotic activity in response to H2O2-induced apoptosis. J Biol Chem 283, 15359–69 (2008). [PubMed: 18344566]
14. Luanpitpong S et al. Regulation of apoptosis by Bcl-2 cysteine oxidation in human lung epithelial cells. Mol Biol Cell 24, 858–69 (2013). [PubMed: 23363601]
15. Azad N et al. S-nitrosylation of Bcl-2 inhibits its ubiquitin-proteasomal degradation. A novel antiapoptotic mechanism that suppresses apoptosis. J Biol Chem 281, 34124–34 (2006). [PubMed: 16980304]
16. Lee S et al. Allosteric inhibition of antiapoptotic MCL-1. Nat Struct Mol Biol 23, 600–7 (2016). [PubMed: 27159560]
17. Guerra RM et al. Precision Targeting of BFL-1/A1 and an ATM Co-dependency in Human Cancer. Cell Rep 24, 3393–3403 e5 (2018). [PubMed: 30257201]
18. Harvey EP et al. Crystal Structures of Anti-apoptotic BFL-1 and Its Complex with a Covalent Stapled Peptide Inhibitor. Structure 26, 153–160 e4 (2018). [PubMed: 29276033]
19. Huhn AJ, Guerra RM, Harvey EP, Bird GH & Walensky LD Selective Covalent Targeting of Anti-Apoptotic BFL-1 by Cysteine-Reactive Stapled Peptide Inhibitors. Cell Chem Biol 23, 1123–1134 (2016). [PubMed: 27617850]
20. Suzuki M, Youle RJ & Tjandra N Structure of Bax: coregulation of dimer formation and intracellular localization. Cell 103, 645–54 (2000). [PubMed: 11106734]
21. Denisov AY et al. Solution structure of human BCL-w: modulation of ligand binding by the C-terminal helix. J Biol Chem 278, 21124–8 (2003). [PubMed: 12651847]
22. Yao Y et al. Conformation of BCL-XL upon Membrane Integration. J Mol Biol 427, 2262–70 (2015). [PubMed: 25731750]
23. Zhang Y I-TASSER server for protein 3D structure prediction. BMC Bioinformatics 9(2008).
24. Roy A, Kucukural A & Zhang Y I-TASSER: a unified platform for automated protein structure and function prediction. Nat Protoc 5, 725–38 (2010). [PubMed: 20360767]
25. Yang J et al. The I-TASSER Suite: protein structure and function prediction. Nat Methods 12, 7–8 (2015). [PubMed: 25549265]
26. Mohanasundaram KA et al. Potential role of glutathione in evolution of thiol-based redox signaling sites in proteins. Front Pharmacol 6, 1 (2015). [PubMed: 25805991]

27. Edlich F et al. Bcl-x(L) retrotranslocates Bax from the mitochondria into the cytosol. Cell 145, 104–16 (2011). [PubMed: 21458670]
28. Herman MD et al. Completing the family portrait of the anti-apoptotic Bcl-2 proteins: crystal structure of human Bfl-1 in complex with Bim. FEBS Lett 582, 3590–4 (2008). [PubMed: 18812174]
29. Hinds MG et al. The structure of Bcl-w reveals a role for the C-terminal residues in modulating biological activity. EMBO J 22, 1497–507 (2003). [PubMed: 12660157]
30. Walensky LD et al. A stapled BID BH3 helix directly binds and activates BAX. Mol Cell 24, 199–210 (2006). [PubMed: 17052454]
31. Lovell JF et al. Membrane binding by tBid initiates an ordered series of events culminating in membrane permeabilization by Bax. Cell 135, 1074–84 (2008). [PubMed: 19062087]
32. Brien G et al. C-terminal residues regulate localization and function of the antiapoptotic protein Bfl-1. J Biol Chem 284, 30257–63 (2009). [PubMed: 19759007]
33. Ottina E, Tischner D, Herold MJ & Villunger A A1/Bfl-1 in leukocyte development and cell death. Exp Cell Res 318, 1291–303 (2012). [PubMed: 22342458]
34. Schenk RL et al. Characterisation of mice lacking all functional isoforms of the pro-survival BCL-2 family member A1 reveals minor defects in the haematopoietic compartment. Cell Death Differ 24, 534–545 (2017). [PubMed: 28085150]
35. Yecies D, Carlson NE, Deng J & Letai A Acquired resistance to ABT-737 in lymphoma cells that up-regulate MCL-1 and BFL-1. Blood 115, 3304–13 (2010). [PubMed: 20197552]
36. Beroukhim R et al. The landscape of somatic copy-number alteration across human cancers. Nature 463, 899–905 (2010). [PubMed: 20164920]
37. Fan G et al. Defective ubiquitin-mediated degradation of antiapoptotic Bfl-1 predisposes to lymphoma. Blood 115, 3559–69 (2010). [PubMed: 20185581]
38. Haq R et al. BCL2A1 is a lineage-specific antiapoptotic melanoma oncogene that confers resistance to BRAF inhibition. Proc Natl Acad Sci U S A 110, 4321–6 (2013). [PubMed: 23447565]
39. Esteve-Arenys A et al. The BET bromodomain inhibitor CPI203 overcomes resistance to ABT-199 (venetoclax) by downregulation of BFL-1/A1 in in vitro and in vivo models of MYC+/BCL2+ double hit lymphoma. Oncogene 37, 1830–1844 (2018). [PubMed: 29353886]
40. Kutuk O & Letai A Regulation of Bcl-2 family proteins by posttranslational modifications. Curr Mol Med 8, 102–18 (2008). [PubMed: 18336291]
41. Mason KD et al. Programmed anuclear cell death delimits platelet life span. Cell 128, 1173–86 (2007). [PubMed: 17382885]
42. Souers AJ et al. ABT-199, a potent and selective BCL-2 inhibitor, achieves antitumor activity while sparing platelets. Nat Med 19, 202–8 (2013). [PubMed: 23291630]
43. Kotschy A et al. The MCL1 inhibitor S63845 is tolerable and effective in diverse cancer models. Nature 538, 477–482 (2016). [PubMed: 27760111]
44. Bechtel TJ & Weerapana E From structure to redox: The diverse functional roles of disulfides and implications in disease. Proteomics 17(2017).
45. Fra A, Yoboue ED & Sitia R Cysteines as Redox Molecular Switches and Targets of Disease. Front Mol Neurosci 10, 167 (2017). [PubMed: 28634440]
46. Harvey EP et al. Identification of a Covalent Molecular Inhibitor of Anti-apoptotic BFL-1 by Disulfide Tethering. Cell Chem Biol (2020).
47. Pitter K, Bernal F, Labelle J & Walensky LD Dissection of the BCL-2 family signaling network with stabilized alpha-helices of BCL-2 domains. Methods Enzymol 446, 387–408 (2008). [PubMed: 18603135]
48. Letunic I & Bork P Interactive Tree Of Life (iTOL): an online tool for phylogenetic tree display and annotation. Bioinformatics 23, 127–8 (2007). [PubMed: 17050570]
49. Barclay LA et al. Inhibition of Pro-apoptotic BAX by a noncanonical interaction mechanism. Mol Cell 57, 873–886 (2015). [PubMed: 25684204]
50. Wales TE & Engen JR Hydrogen exchange mass spectrometry for the analysis of protein dynamics. Mass Spectrom Rev 25, 158–70 (2006). [PubMed: 16208684]

51. Perez-Riverol Y et al. The PRIDE database and related tools and resources in 2019: improving support for quantification data. Nucleic Acids Res 47, D442–D450 (2019). [PubMed: 30395289]

52. Cohen NA et al. A competitive stapled peptide screen identifies a selective small molecule that overcomes MCL-1-dependent leukemia cell survival. Chem Biol 19, 1175–86 (2012). [PubMed: 22999885]

53. Leshchiner ES, Braun CR, Bird GH & Walensky LD Direct activation of full-length proapoptotic BAK. Proc Natl Acad Sci U S A 110, E986–95 (2013). [PubMed: 23404709]

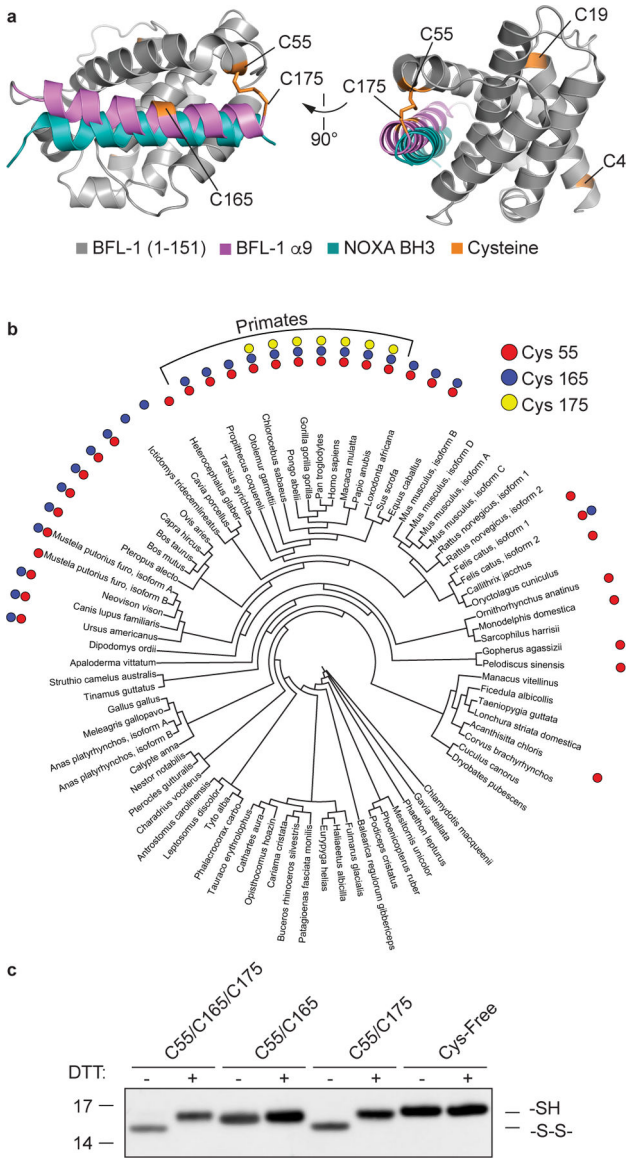

Figure 1. A covalent α9-in-groove interaction is mediated by C55 and C175 of BFL-1.

(a) Comparison of a full-length model structure of BFL-1 generated by I-TASSER and the crystal structure of the complex between BFL-1ΔC and a NOXA BH3 helix (cyan; PDB ID: 3MQP). The I-TASSER model predicts an intramolecular disulfide bond between C55 of the BH3-binding groove and C175 of α9 (purple) in full-length BFL-1. (b) The presence or absence of cysteines 55, 165, and/or 175 are indicated across all annotated BFL-1 sequences in the unscaled phylogenetic tree. The co-existence of C55 and C175 emerged in primates. A full sequence alignment and UniProt IDs can be found in Supplementary Data File 1. (c) Electrophoretic mobility of the indicated recombinant BFL-1 constructs with and without DTT pre-treatment. Those constructs that retain C55 and C175, and not exposed to reducing conditions, display a faster-migrating species consistent with the lower hydrodynamic radius that results from intramolecular disulfide bond formation. The uncropped image for panel c is available online.

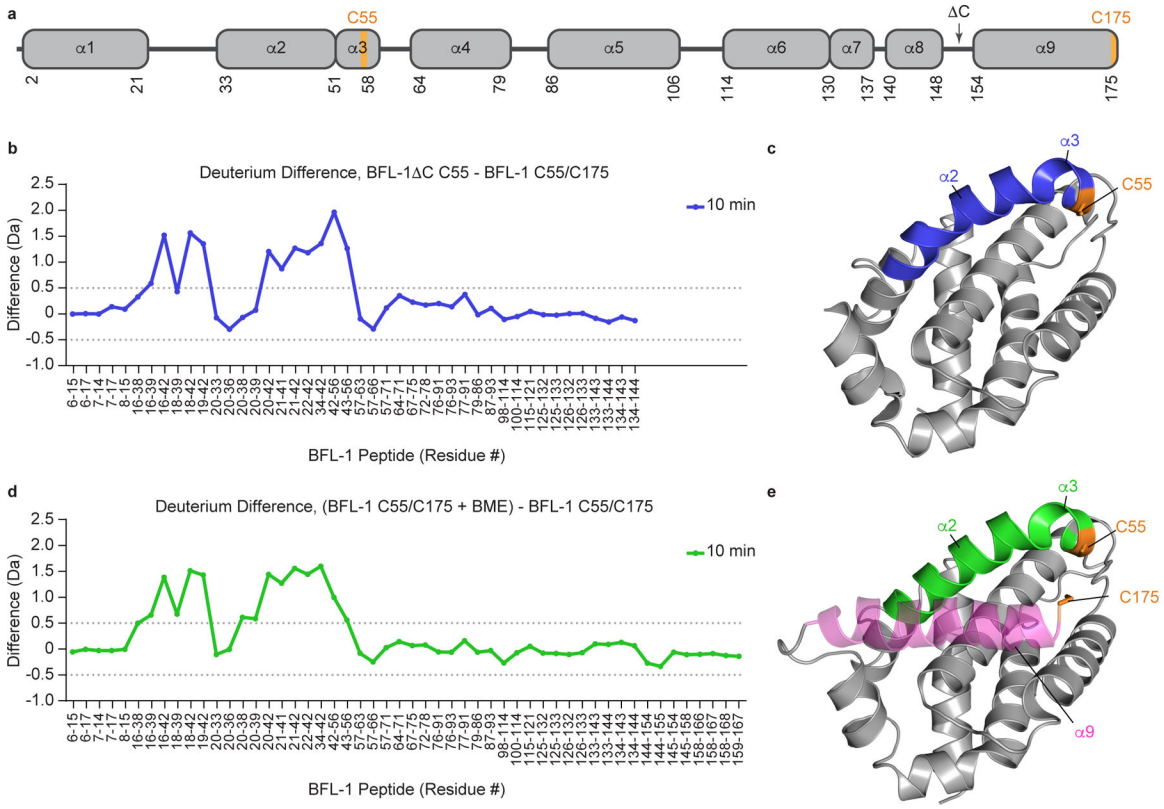

Figure 2. A redox switch controls α9 occupancy of BFL-1's canonical groove.

(a) Domain map of full-length BFL-1 highlighting the amino acid sequences that correspond to the individual α-helices, the truncation site for BFL-1ΔC C55, and the locations of C55 and C175 (colored in orange). (b) A deuterium difference plot showing the relative deuterium incorporation of BFL-1ΔC C55 minus the relative deuterium incorporation of full-length BFL-1 C55/C175, as measured at 10 minutes of deuterium labeling. Compared to BFL-1 C55/C175, α-helices 2 and 3, which comprise a surface of the BH3-binding groove, are relatively deprotected in BFL-1ΔC, which lacks α9. Data are representative of three independent experiments for each protein (Supplementary Table 1). (c) The α2 and α3 regions of deprotection (blue) in the absence of α9 are mapped onto the structure of BFL-1ΔC (PDB ID: 5WHH). (d) A deuterium difference plot showing the relative deuterium incorporation of full-length BFL-1 C55/C175 in the presence of BME minus the relative deuterium incorporation of full-length BFL-1 C55/C175 in the absence of BME, as measured at 10 minutes of deuterium labeling. Data are representative of two independent experiments for BME-reduced BFL-1 C55/C175 and three independent experiments for BFL-1 C55/C175 (Supplementary Table 1). (e) The α2 and α3 regions of deprotection (green) are mapped onto the model structure of reduced BFL-1 C55/C175 (I-TASSER) with the simulated α9 helix colored in magenta. All HXMS data used to create this figure can be found in Supplementary Data File 2.

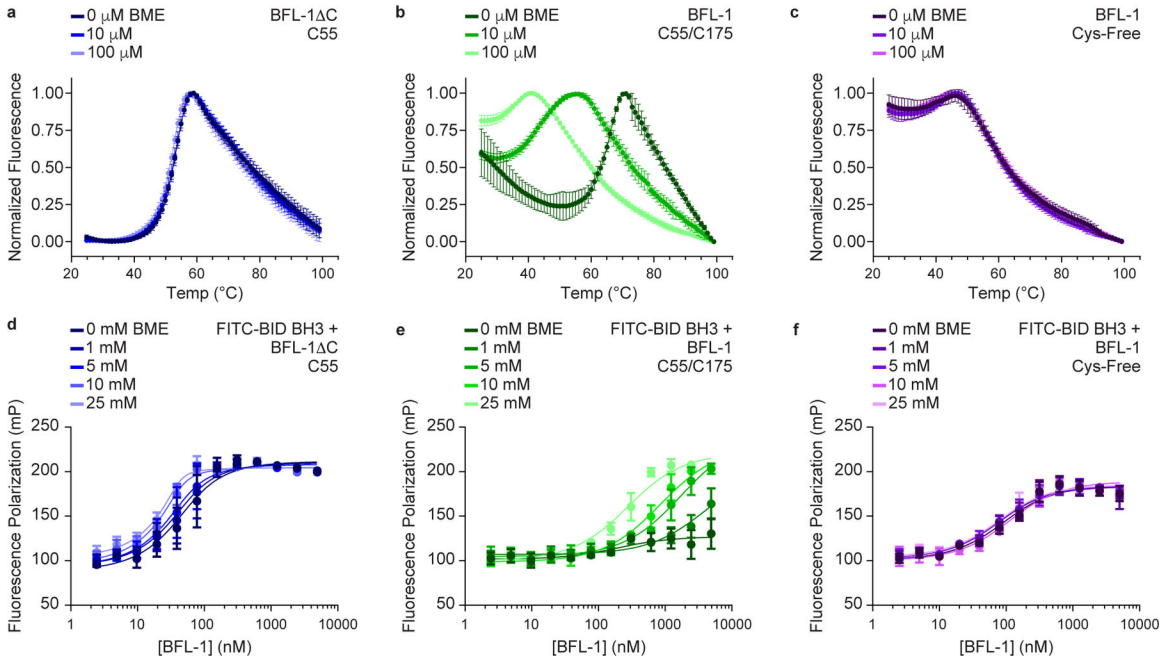

Figure 3. Disulfide formation regulates the stability and BH3-binding activity of BFL-1.

(a-c) Thermal denaturation curves as measured by differential scanning fluorimetry (DSF) of the indicated BFL-1 proteins (5 μM protein), BFL-1ΔC C55 (a), BFL-1 C55/C175 (b), and BFL-1 Cys-free (c), in the absence and presence of increasing concentrations of BME. Data are mean ± S.D. for experiments performed in technical octuplicate. The plots are representatives of two biological replicates performed with independent preparations of protein. (d-f) Fluorescence polarization (FP) assays measuring the direct interaction between FITC-BID BH3 peptide (60 nM) and the indicated BFL-1 constructs, BFL-1ΔC C55 (d), BFL-1 C55/C175 (e) and BFL-1 Cys-free (f), in the absence and presence of increasing concentrations of BME. Data are mean ± S.D. for experiments performed in technical quadruplicate. The plots are representatives of two biological replicates performed with independent preparations of protein and ligand. Data for the DSF and FP plots are available as Supplementary Data File 3.

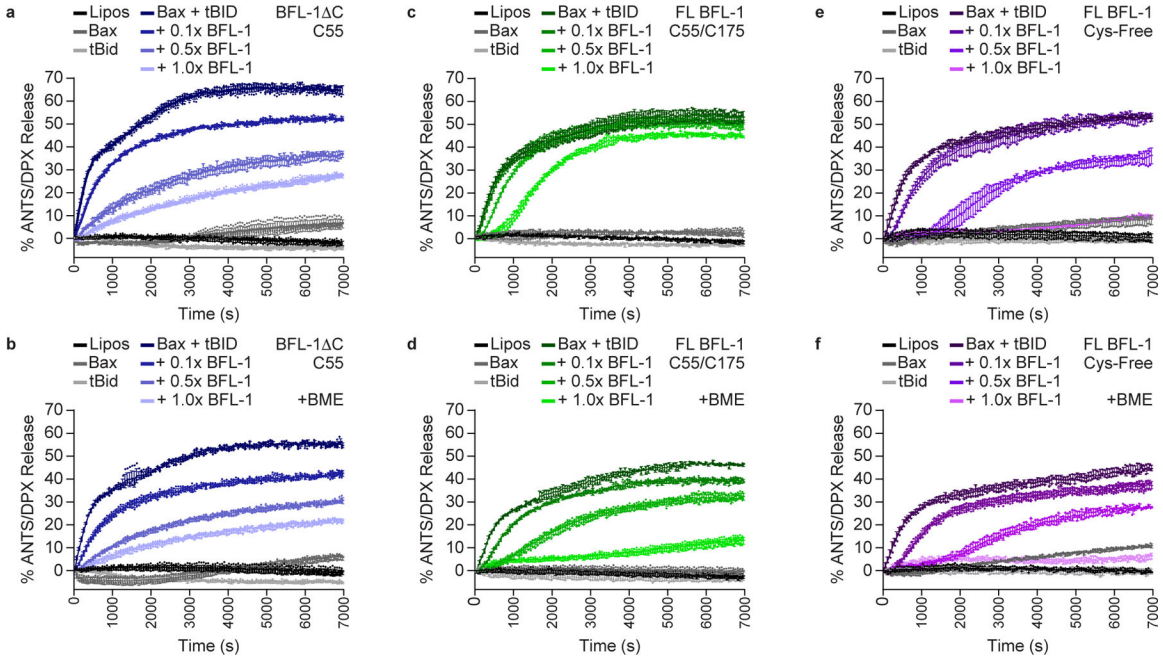

Figure 4. BFL-1 suppression of BAX-mediated membrane permeabilization is regulated by the disposition of its α9 domain.

(a-f) The effect of BME on the capacity of BFL-1 proteins (0, 50, 250, 500 nM), BFL-1ΔC C55 (a, no BME; b, with BME), BFL-1 C55/C175 (c, no BME; d, with BME), or BFL-1 Cys-free (e, no BME; f, with BME), to block tBID (20 nM)-triggered, BAX (500 nM)-mediated membrane permeabilization was evaluated by liposomal release assay. Data are mean ± S.D. for experiments performed in technical triplicate. These experiments were repeated three times using independent preparations of liposomes and proteins with similar results. Source data for the liposomal release assay plots are available online.

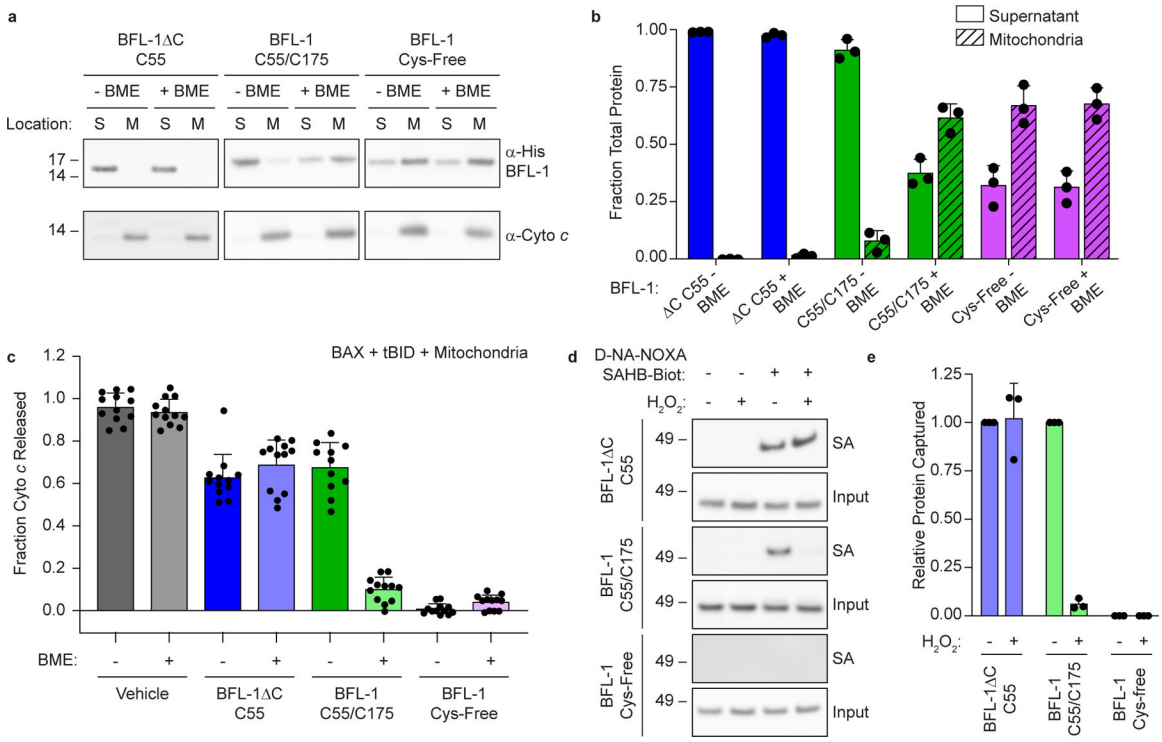

Figure 5. A C55-C175 redox switch controls BFL-1 translocation and membrane-protection in isolated mitochondria and the BH3-binding functionality of BFL-1 in cells.

(a) Relative distribution of the indicated BFL-1 constructs (1 μM) between supernatant (S) and BAX/BAK-deficient mitochondrial fractions (M) in the absence and presence of BME, as detected by His_6 western analysis. Cytochrome *c* western analysis was performed to confirm the identity of the intact mitochondrial fraction. The experiment was performed three times using independent protein and mitochondrial preparations with a representative replicate shown. (b) Distribution of the indicated BFL-1 constructs between supernatant and mitochondrial fractions (a) was quantified using ImageJ software. Data are mean ± S.D. of three independent replicates using freshly prepared protein and mitochondria. (c) Cytochrome *c* (Cyto *c*) release from BAX and BAK-deficient mitochondria into the supernatant in response to incubation with tBID (10 nM), BAX (100 nM), and the indicated BFL-1 constructs (100 nM), in the absence and presence of BME (50 μM), as measured by ELISA. Data are mean ± S.D. for n=12 per condition (4 technical replicates each of three independently performed experiments using freshly prepared protein and mitochondria). (d) The accessibility of the BFL-1 canonical groove for BH3 capture was monitored in cells using a BFL-1-selective covalent BH3-targeting assay. 293T cells expressing the indicated N-terminal GFP-BFL-1 constructs were incubated with or without C-terminally biotinylated D-NA-NOXA SAHB-15 R31E (5 μM) in the absence and presence of sub-cytotoxic hydrogen peroxide (100 μM) for 24 h. Formation of the D-NA-NOXA SAHB-derivatized BFL-1 adduct was detected by streptavidin (SA) pull-down from cellular lysate, followed by electrophoresis and GFP western analysis. The experiment was performed three times using independent cell cultures and a representative replicate is shown for each condition. (e) BH3-capture of expressed BFL-1ΔC, BFL-1 C55/C175, and BFL-1 Cys-free upon treatment of 293T cells with biotinylated D-NA-NOXA SAHB-15 R31E in the presence or absence of

H_2O_2 (100 μM) (d) was quantitated using ImageJ software to determine relative protein capture in the presence vs. absence of peroxide. Data are mean ± S.D. of three independent sets of pull-down experiments. Uncropped images for panels a and d are available online. Source data for mitochondrial translocation, cytochrome *c* release, and formation of D-NA-NOXA SAHB-derivatized BFL-1 in cells are available online.

Table 1.

Melting temperatures of BFL-1 constructs.

The melting temperatures (T_m) of the indicated BFL-1 constructs in the absence and presence of increasing concentrations of BME. Data are the calculated T_m values from the curve fits ± S.E. for experiments performed in technical octuplicate and representative of two biological replicates performed with independent preparations of protein. Data used for T_m calculations are available in Supplementary Data File 3.

	BFL-1 Construct: T_m (°C)		
BME (μM)	**ΔC C55**	**C55/C175**	**Cys-Free**
0	55.5 ± 0.1	65.4 ± 0.3	40.5 ± 2.1
10	52.4 ± 0.1	43.4 ± 0.2	41.6 ± 1.0
100	51.3 ± 0.1	35.1 ± 0.3	38.4 ± 0.4

Table 2.
Dissociation constants for BID BH3 interaction with BFL-1 constructs.

Dissociation constants (K_d) for the binding interactions between the indicated BFL-1 constructs and FITC-BID BH3 (20 nM), as measured by fluorescence polarization assay in the absence and presence of increasing concentrations of BME. Data are the calculated K_d values from the curve fits ± S.E. for experiments performed in technical quadruplicate and representative of two biological replicates performed with independent preparations of protein and ligand. Data used for K_d calculations are available in Supplementary Data File 3.

	BFL-1 Construct: K_d (nM)		
BME (mM)	**ΔC C55**	**C55/C175**	**Cys-Free**
0	24.3 ± 6.4	> 2000	68.8 ± 14.0
1	18.4 ± 5.1	> 2000	55.1 ± 12.6
5	12.3 ± 3.7	1750 ± 376	55.5 ± 10.6
10	3.3 ± 1.1	851 ± 126	89.7 ± 16.0
25	1.6 ± 0.7	259 ± 39	55.9 ± 0.1